First Ground-Based Mapping of the Asteroid Vesta

C. DUMAS (Observatoire de Paris-Meudon (DESPA) and University of Hawaii (IfA))
O.R. HAINAUT (University of Hawaii (IfA))

Asteroid 4 Vesta has been imaged in the Near-Infrared using the ESO 3.6-m telescope equipped with the Come-On-Plus adaptive optics system. The result of these observations is the first mineralogic map of a minor planet obtained from ground-based observations. We will discuss the data acquisition and reduction techniques that we used and developed, and present our ground-based observational prospects.

1. Introduction: Vesta

With a mean diameter of 520 km[20], Vesta is the third largest asteroid. Its orbit is located in the Main Belt, at 2.4 AU from the Sun. Its surface albedo is very high (0.38) compared to other asteroids whose albedo does usually not exceed 0.15. Vesta is large enough to have experienced a differentiation phase during its accretion: the heaviest elements like Iron separated to sink towards the core of the primordial body. While it cooled down, basaltic lava flows erupted on Vesta's surface through the cracks in the forming crust. At that time, highly energetic collisions between asteroids were very frequent, redistributing the material all over the surface. Previous observations[2,10,18,19] showed that the surface of most of the minor planets appears uniform, with little or no albedo variation. Surprisingly, spectrophotometric observations of Vesta[15] revealed a spectrum dominated by some strong absorption bands whose intensity varies with the rotation of the asteroid[9], implying that the surface of Vesta has some dark and bright areas. The dark regions are interpreted as some old material darkened by the erosion processes (solar wind and photo-dissociation) over its lifetime, while the brighter spots are considered to be some fresher material excavated by cratering impacts with smaller bodies. During such impacts, some fragments reached a sufficient velocity to escape the gravitational field of Vesta and be released in the inner solar system. It is generally accepted that these fragments are at the origin of the basaltic achondrite (HED) meteorites[15].

With the availability of the Hubble Space Telescope and its corrected optics, and with the development of Adaptive Optics on telescopes of the 4-m class, we are now able to obtain direct images resolving the disk of the biggest asteroids. Speckle Interferometry provides a similar resolving power[5], but requires extremely heavy and complex image reconstruction techniques. The original goal of our AO observations was to obtain resolved images of the whole visible surface of Vesta at 12 wavelengths sampling the 2.0 μm pyroxene band. Constraining this dataset with the spectra obtained from laboratory samples of HED meteorites, we would have obtained some crucial indications on the distribution of the pyroxene band strength, on the pyroxene chemical composition and grain size distribution[11]. The location of the impacting zones on Vesta could then have been determined with a very high accuracy, leading to a better understanding of the chemical and physical processes undergone by Vesta during its lifetime.

2. Observations

During its December 1994 opposition, we observed Vesta in the Near-Infrared with Come-On-Plus (CO+). The images were obtained on the Nicmos SHARP II camera through a Continuously Variable Filter ($\lambda/\Delta\lambda \simeq 60$). The pixel size was 0.05″, ensuring us a sufficient sampling of the image in order to satisfy the Shanon's principle. We did not select a smaller pixel size because the broad "wings" of the objects would not have fit in the corresponding field. At the time of the observations, the inclination of Vesta's rotational axis with respect to the line of sight was such that we could see almost 80% of its surface during an entire rotation period. Its angular diameter was 0.44″, almost 9 pixels across the chip. Because of some scheduling conflicts we could not observe Vesta during its transit, but only after, when it was at higher airmasses, pushing CO+ beyond its nominal limit of 60° of zenithal distance. We could only secure 3^h50^{min} of data, instead of the 10^h originally attributed to achieve our goals. Moreover, the

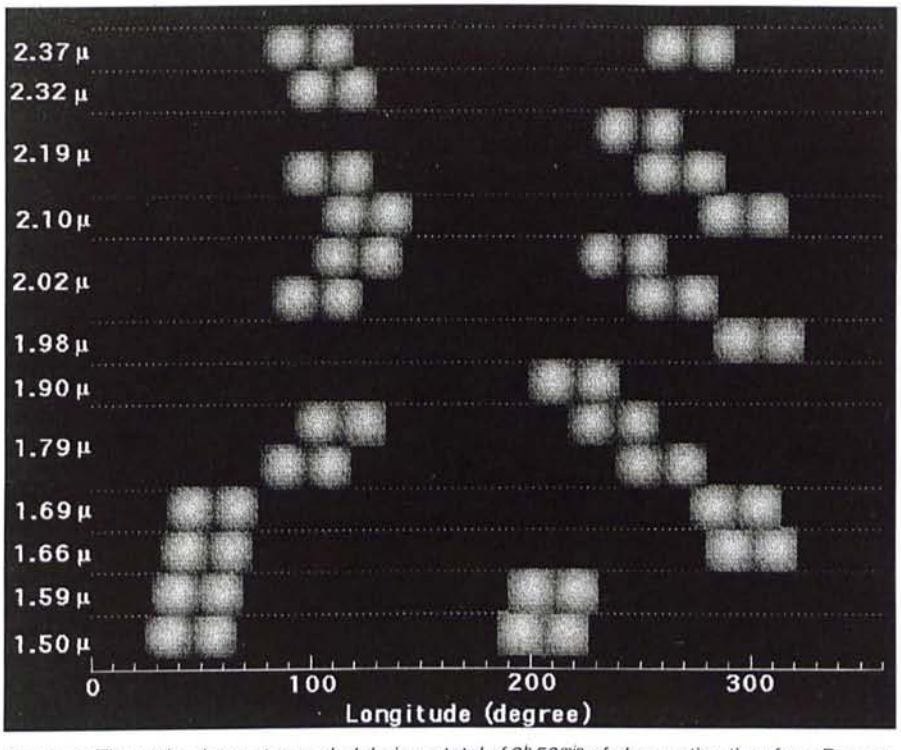

Figure 1: The entire data set recorded during a total of 3^h50^{min} of observation time from December 9–13, 1994. The x-abscissa is the central longitude of Vesta and the y-abscissa is the wavelength of the CVF at which Vesta was imaged. For each exposure, we obtain two images. The images shown are the raw images, i.e. no restoration has yet been applied to recover the optimal resolution of the instrument. We have recorded images at different wavelengths, from 1.5 to 2.37 μm, in order to scan the 2.0 μm pyroxene band. We do not have a complete longitudinal coverage of Vesta. Our images are roughly centred on the Vesta longitude 100° and 250°. Some features at the surface are already visible in the raw images. The rotation period of Vesta is 5.3^h and its angular diameter was 0.44″ for the 1994 opposition.

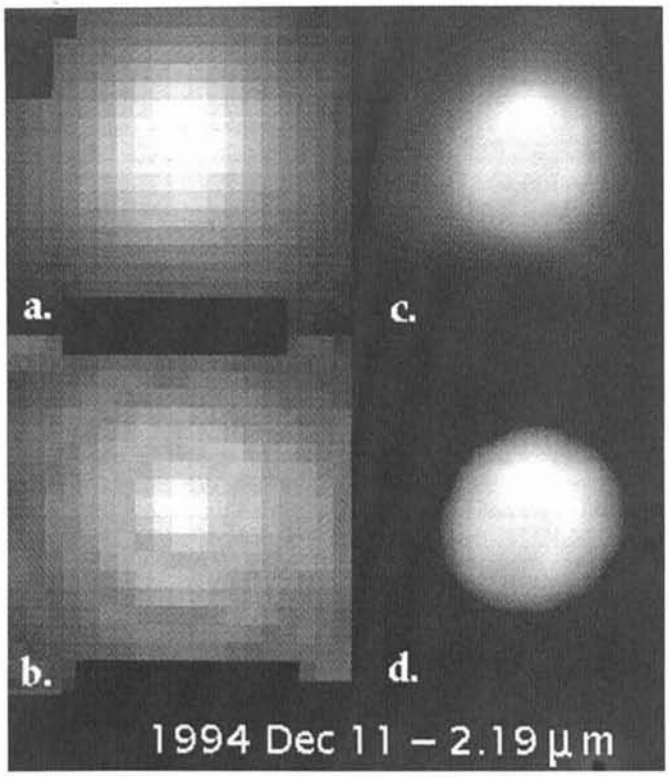

Figure 2:
– a: raw image
– b: PSF (logarithm grey-scale)
– c: Vesta image deconvolved by Lucy-Richardson (50 iterations)
– d: result of the wavelet transformation applied to the raw image. There is an excellent agreement between the result of Lucy-Richardson deconvolution (which use a PSF) and the wavelet transformation (simple spatial filtering).

weather was far from ideal (poor seeing and/or non photometric) during 3 of the 4 nights when we observed, and finally the camera displayed a systematic pattern noise. As a consequence, the dataset (illustrated in Fig. 1) does not cover the whole visible surface, and the regions observed do not have an equal coverage in wavelength. In order to establish a map of Vesta we had to combine some images recorded at different wavelengths. This has the same disturbing effect as looking at a landscape through a stained glass window. Each observation of Vesta consisted in a series of 30–50 short exposures (5 sec each) obtained in two different quadrants of the SHARP II camera, ensuring that the minor planet and the background are recorded simultaneously. We also obtained images of the solar-type star SAO 78355, which was chosen for its angular proximity to Vesta and its magnitude close to that of our object, in order to be used as reference Point-Spread-Function for further deconvolution, as well as a rough photometric calibrator.

3. Data Reduction

A bad pixel map was produced for each night, and the corresponding pixels were interpolated over in every individual image. For each object (Vesta and star) the data are distributed in two "cubes" of images: two object-cubes and two sky-cubes, one for each quadrant used during the exposure. For each quadrant, a unique sky frame is obtained by taking the median of the sky-cube. This sky frame is then subtracted from each image of the corresponding object-cube. Images of the dome were obtained through the same CVF. They were normalised and combined to generate a template flat-field, which is applied to each image of the data cube. However, we do not have suitable frames at each of our wavelength. We then found that the short-scale structures do not change much with the wavelength in the 1.5–2.5 µm range, allowing us to use the flat-fields obtained at a nearby wavelength. Each object image is then recentred on the central pixel of the frame. This is performed by zeroing the average phase of the image in the Fourier space. This technique proved to be much more accurate than the methods based on the centre-of-mass determination. Once the centring is done, we average the object cube in order to get a final and unique image for each quadrant. For every wavelength we end up with a set of two images of Vesta and two images of the star. In what follows, we refer to these as "raw images", in the sense that only the standard processing and no restoration technique has been applied. The images containing a pattern of systematic noise (induced by the reading of the camera) at a non-negligible level, have been filtered in the Fourier space[21].

None of the four nights was photometric, therefore no spectrophotometric calibration star was imaged. The images have been calibrated relatively to each other by adjusting the total integrated flux of each raw image to the measured flux of a spectrum of Vesta at the same wavelength.

To recover the optimal image resolution, we applied different restoration techniques:

– *Wiener filtering*, which is a simple division of the object by the PSF in the Fourier space, taking in account a certain level of noise present in the images.

– *Richardson-Lucy deconvolution*, using a new-generation algorithm by Hook and Lucy[1] based on an iterative maximum likelihood optimisation. We performed some tests on synthetic and real images of Vesta and of the PSF. They show that the best restoration is obtained after 50 iterations. A smaller number of iterations does not restore all the details of the image, while continuing over 50 iterations tends to create a "hole" in the centre of the minor planet disk and enhance its limb.

– *Wavelets spatial filtering*: the image is transformed in the wavelet space[16], from which some spatial frequencies are extracted to build the restored images. The advantage of this technique is that it does not require a PSF. It should how-

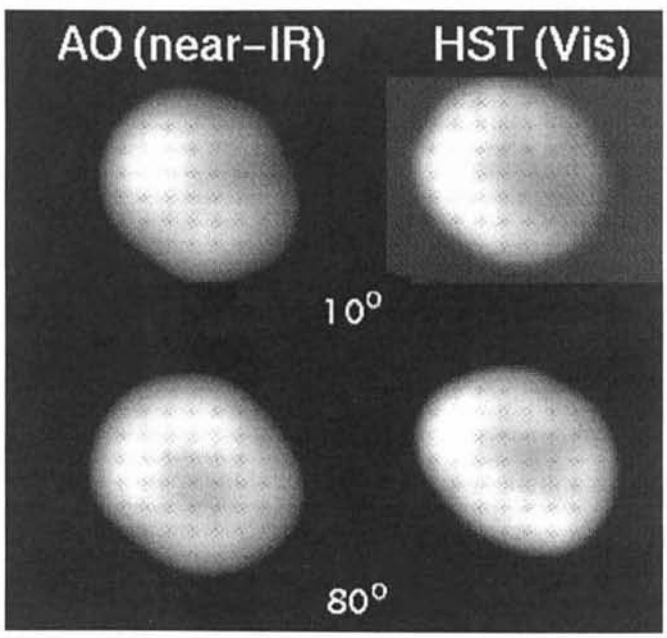

Figure 3: Adaptive Optics observations of Vesta from ESO (near-infrared) and HST (visible) – (Zellner B., Storr A., priv. comm.). These two images were recorded at nearly the same central longitude. The overall shape of the asteroid is the same as well as the main albedo features. On the AO images, Vesta is about 9 pixels across the chip. The AO images have been deconvolved using 50 iterations of the Lucy-Richardson algorithm.

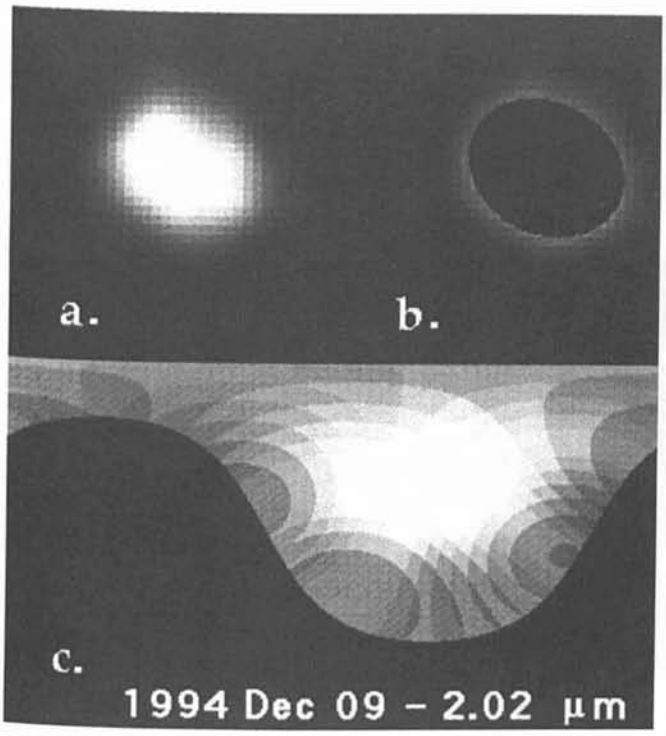

Figure 4: The map extraction is done by assuming a spheroidal shape for Vesta, with a ratio of 1.2 between the two diameters.
– a: image of Vesta after 50 iterations of Lucy-Richardson
– b: residual after subtraction of the spheroidal model
– c: map extracted. Similar maps were produced for all the images of our data set. During the 1994 opposition only 80% of Vesta's surface was visible. The unseen regions are black. Note the limb darkening present in the extracted map.

ever be noted that the enhancement in resolution achieved by this technique is not as good as that of the Lucy deconvolution.

The data have been processed using the Interactive Data Language (IDL), except the wavelet restoration which was performed with the ESO-MIDAS "wavelets" context. The results of these three restoration techniques show an excellent agreement in most cases (Fig. 2) – the disagreeing ones can all be explained either by a very bad raw image of Vesta, or a bad PSF. We are therefore confident that the features seen on Vesta are not artifacts introduced during the restoration process but rather some real albedo variations over the surface, due to some change in the nature of the minerals that form the asteroid regolith. It is interesting to note that HST observed Vesta nearly simultaneously in the visible wavelengths (WFPC Zellner et al., FOC Albrecht et al.). The WFPC team kindly made their raw and restored images available to our group, allowing us to compare our results. Figure 3 shows the comparison of HST (visible) and ESO (near-infrared) Vesta images recorded at nearly the same central longitude of the asteroid. Although some differences have to be expected because of the different wavelength ranges, the main albedo features are identical as well as the overall shape of the asteroid. As the instrumental set-up was completely different and the data processing totally independent, we take this as an additional confirmation of the reality of these features.

We extracted a map from each Vesta image by modelling the minor planet with an oblate spheroid whose eccentricity was adjusted to fit the images (Fig. 4). We used the orientation of the rotation axis set in the Magnusson's synthesis of the published pole solutions[14]. Our data are in perfect agreement with that orientation but cannot refine it. The local divergence of Vesta with a pure ellipsoid will produce some errors in the projection for the region close to the limb. As described later, this portion of the images is not taken into account in the final map and therefore is of little consequence. It should be noted that one single pixel on a Vesta image may be projected into an area that strongly varies depending on the angle θ between the normal to the surface of the asteroid and the line of sight. More specifically, a pixel close to the limb will correspond to a huge region of the minor planet that is seen in very poor conditions. This effect is taken into account by affecting a "weight" to each data-point: this weight is maximum for the sub-Earth pixel, and is equal to zero for the pixels where $\theta = 90°$. Each individual map is corrected for the limb darkening effect, using a simple $\cos(\theta)^{\kappa}$ law[4], where the exponent κ is adjusted to the data. This simple correction tends to over-correct the extreme edges of the limb, and will have to be refined. The final maps are obtained by taking the weighted median of the individual maps.

4. Results

Since our longitudinal coverage is not complete, we cannot confirm the triaxial shape measured from speckle interferometry[6] and HST[20] . But the two diameters measured from our images are in very good agreement with the HST measurements (560 km × 450 km). As mentioned before, we could not obtain a complete longitude coverage of Vesta at each wavelength. Still, a rough estimate of the pyroxene distribution can be assessed by combining all the data into two maps – the first one summing all the individual maps obtained at wavelengths outside the pyroxene band – the second, all those obtained inside the band. These two maps are reproduced in Figure 5. The black area corresponds to some "Terra Incognita" that was not visible at the time of the observations. It must be noted that, because we could not obtain a good coverage of Vesta, the reliability of the map varies much with the longitude. The regions of the map around 90° and 270° have been imaged several times and can be relied on, while the regions around 0° and even more around 180° are built from just a few pixels close to the limb. In a similar way, the maps of the regions below –15° and over 80° of latitude are not reliable. Among the features visible in the reliable parts of the maps, there is a strong albedo variation from one hemisphere to the other, variation even enhanced on the map corresponding to wavelengths in the bottom of the pyroxene band. This confirms previous photometric observations of the existence of a dark and a bright hemisphere on Vesta[3]. The difference of contrast between these two hemispheres from one map to the other indicates an enhancement of the pyroxene content of the left hemisphere (longitude below 180°) . Smaller details can be seen: the left hemisphere shows for example two bright spots separated by a dark region. Also the bright area visible on the right hemisphere is elongated and might correspond to a large impact zone on Vesta. A more detailed analysis of these maps is beyond the scope of this paper, and will be given in Dumas and Hainaut (1996).

The most encouraging result remains that even with poor seeing and weather, at high airmass and during a non-optimal opposition, we could obtain such a detailed map. The next step is of course to complete the pyroxene map of Vesta, and to extend it to the feldspar and olivine bands. The May 1996 opposition is one of the most favourable in terms of angular diameter (0.65″, 1.4 × its diameter in 1994) and aspect angle (more than 99% of the surface will be visible). We also wish to extend this programme to Ceres and Pallas in order to map the water of hydration that their surface is suspected to have retained since the asteroid belt formed[13]. Also in the case of Ceres some observational results[12] and calculations[8] sustain the fact that this asteroid might have some polar caps whose thickness varies with the seasonal variations induced by the inclination of its rotation axis[17]. Ceres and Pallas will be at opposition at about the same time as Vesta, making of May 1996 a fantastic period for the study of asteroid mineralogy. Unfortunately, no time was allo-

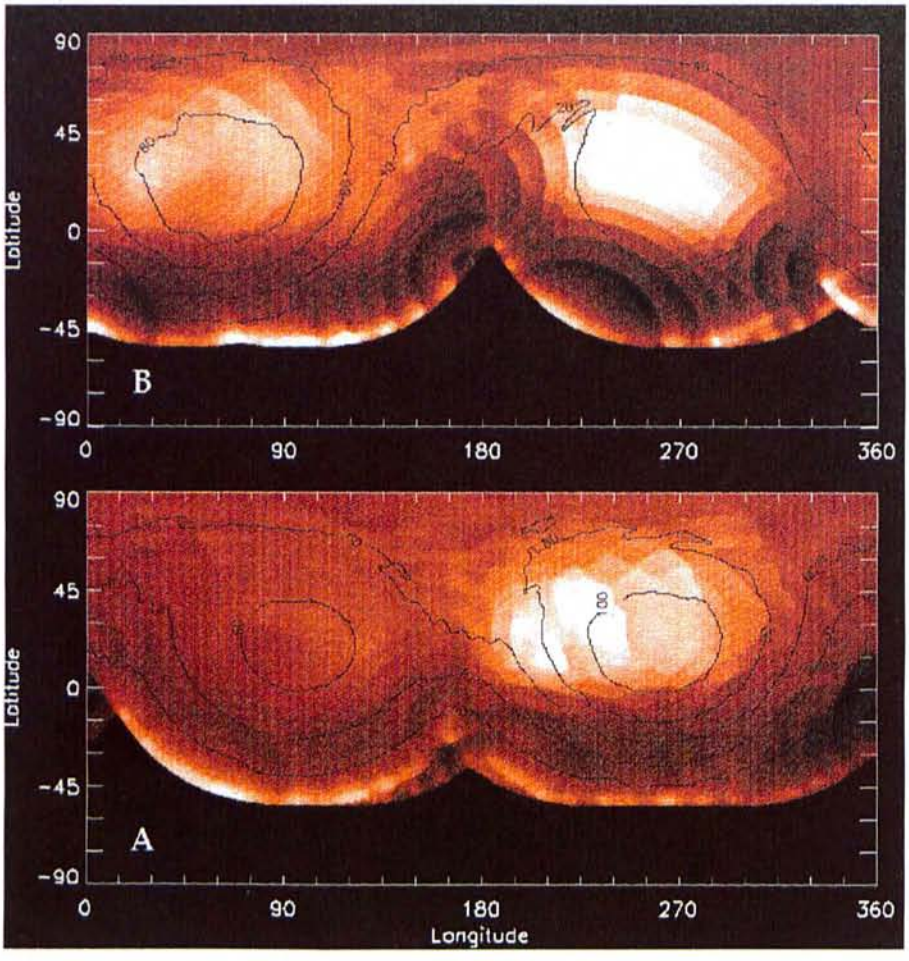

Figure 5: Map of the pyroxene distribution on Vesta. This is the first mineralogic map of Vesta based on direct observations. Map A: extracted from the images whose wavelength corresponds to the bottom of the pyroxene band. Map B: extracted from the images whose wavelength is outside the pyroxene band. The contour level is a measurement of the reliability of the data. The correction of the limb darkening introduces an artificial enhancement in the intensity of the two maps close to the limb. Map A shows clearly the existence of a pyroxene dominated hemisphere on Vesta (for longitude below 180°). This hemisphere becomes bright in the top map corresponding to the spectral range outside the pyroxene band. Some smaller structures are visible in each hemisphere. The range below –15° and above +80° of latitude, should be considered with caution since these data result from pixels located close to the limb of Vesta. Also, our longitudinal coverage being incomplete, the points on these maps close to longitude 0° and 180° have been obtained only from a small number of pixels, also localised close to the limb. Considering the bottom map, the bright hemisphere might correspond to a region where the largest number of impacts on Vesta occurred, the dark hemisphere to some older material, unaltered since the Vesta formation.

cated for this programme at ESO, and we will not be able to test the capabilities of ADONIS (Come-On-Plus' upgrade) under such good conditions before a long time (e.g. July 2000 will be almost as good for Vesta). ADONIS is the best instrument available to carry out this programme, thanks to the large spectral coverage offered by its cameras (COMIC, sensitive from 1.0 to 5.0 μm and an upgraded version of SHARP II), and the possibility to use a CVF. This programme was awarded one night on the Canada-France-Hawaii Telescope. The infrared camera used with this instrument is not sensitive above 2.5 μm and it is not equipped with a CVF. Despite a too short allocated time to complete our scientific objectives, these observations will refine the current map of Vesta and perform some exploratory observations of the water distribution over Ceres and Pallas.

Acknowledgements

We are very grateful to R. Albrecht, H. Schobert and the COME-ON+ team for their help at the telescope during the observations, B. Zellner for keeping us informed of the results of his team and giving us access to the HST images of Vesta, A. Barucci and D. Jewitt for kindly reviewing this article and for all the improvements they suggested, C. Roddier for her precious advise regarding the image analysis techniques we used, T. Encrenaz and T. Owen for their support during all these months spent working on this project and for their suggestions and encouragements concerning the future of this programme.

References

[1] Adorf, H. M. 1990, *ST-ECF Newsletter* **14**, 8–12.
[2] Albrecht, R. 1992, "HST Observations of 1 Ceres", *BAAS* **24** (3), 970.
[3] Bobrovnikoff, N. T. 1929, "The Spectra of Minor Planets", *Lick Obs. Bull.* **14**, 18–27.
[4] Buil, C. 1991, "CCD Astronomy", 209, Willmann-Bell, Richmond.
[5] Drummond, J.D., E.K. Hege 1989, "Speckle Interferometry of Asteroids", in *Asteroids II* (R. P. Binzel, T. Gehrels, M. S. Matthews Eds), 171–191, Univ. of Arizona Press, Tucson.
[6] Drummond, J., A. Eckart, E.K. Hege 1988, "Speckle Interferometry of Asteroids – IV. Reconstructed Images of 4 Vesta", *Icarus* **73**, 1–14.
[7] Dumas, C., O.R. Hainaut 1996, "Ground-Based Mapping of the Asteroid 4 Vesta" (in preparation to be submitted to *Icarus*).
[8] Fanale, F.P., J.R. Salvail 1989, "The Water Regime of Asteroid 1 Ceres", *Icarus* **82**, 87–110.
[9] Gaffey, M. J., W. Hall 1995, "Surface Lithogic Heterogeneity of Asteroid 4 Vesta", submitted to *Icarus*.
[10] Hainaut, O. 1994, thesis dissertation, Université de Liège and ESO, 154–161.
[11] Hiroi, T., R.P. Binzel, J.M. Sunshine C. M. Pieters, H. Takeda 1995, "Grain Sizes and Mineral Compositions of Surface regoliths of Vesta-Like Asteroids", *Icarus* **115**, 374–386.
[12] Lebofsky, L.A., M.A. Feierberg, A.T. Tokunaga, H.P. Larson, J.R. Johnson 1981, "The 1.7 μm – 4.2 μm Spectrum of Asteroid 1 Ceres: Evidence for Structural Water in Clay Minerals", *Icarus* **48**, 453–459.
[13] Lebofsky, L.A. 1980, "Infrared Reflectance Spectra of Asteroids: a Search for Water of Hydration", *Astron.J.* **85**, 573–585.
[14] Magnusson, P. 1989, "Pole Determinations of Asteroids", in *Asteroids II* (R.P. Binzel, T. Gehrels, M.S. Matthews Eds), 1180–1190, Univ. of Arizona Press, Tucson.
[15] McCord, T.B., J.B. Adams, T.V. Thomson 1970, "Asteroid Vesta: Spectral Reflectivity and Compositional Implications", *Science* **168**, 1445–1447.
[16] Meyer, Y. 1989, "Wavelets", Combes J. M. et al. Eds, 21, Springer Verlag, Berlin.
[17] Millis, R.L., L.H. Wasserman, O.G. Franz, R.A. Nye et al. 1987, "The Size, Shape, Density, and Albedo of Ceres from its Occultation of BD+8.471°", *Icarus* **72**, 507–518.
[18] St Pé, O., M. Combes, F. Ribaut, Tomasko M., Fulchignoni M. 1993, "Demonstration of Adaptive Optics for Resolved Imagery of Solar System Objects: Preliminary Results on Pallas and Titan", *Icarus* **105**, 263–270.
[19] St Pé, O., M. Combes, F. Ribaut 1993, "Ceres Surface Properties by High-Resolution Imaging from Earth", *Icarus* **105**, 271–281.
[20] Thomas, P.C., R.P. Binzel, M.J. Gaffey, A. Storrs, E.N. Wells, B. Zellner, 1995, "Vesta: HST Observations of Shape, Spin Pole and Surface Features", Abstract DPS Meeting.
[21] Wampler, E.J. 1992, "FFT Removal of Pattern Noise in CCD Images", *The Messenger* **70**, 82.

C. Dumas
e-mail: dumas@galileo.IFA.Hawaii.Edu